2026 Volume: 02 Issue: 11 www.ijrpa.com ISSN 2456-9995 Research Article

International Journal Research Publication Analysis

Page: 01-13

CFD SIMULATION AND COMPARATIVE THERMAL ANALYSIS OF DIFFERENT FIN SHAPES FOR LED HEAT-SINK APPLICATIONS UNDER NATURAL CONVECTION

***[1]Dr. Nitin Namdeo Pawar, [2]Pramod Kashiram Jadhao**

[1]Department of Mechanical Engineering, Adsul Technical Campus Chas Ahilyanagar.

[2]Mechanical Engineering Department. MGM's College of Engineering and Technology, Kamothe, Navi Mumbai.

Article Received: 11 October 2026

Article Revised: 01 November 2026

Published on: 20 November 2026

***Corresponding Author: Dr. Nitin Namdeo Pawar**

Department of Mechanical Engineering, Adsul Technical Campus Chas Ahilyanagar.

DOI: https://doi-doi.org/101555/ijrpa.2326

ABSTRACT

The geometry of heat-sink fins has a major influence on passive thermal management of light-emitting diode (LED) lighting systems. This study presents a comparative numerical framework for evaluating rectangular plate fins, circular pin fins, triangular fins and drop-shaped fins under natural-convection cooling. The configurations are compared under common base dimensions, aluminium material, ambient conditions and a reference thermal load. Temperature distribution, maximum temperature, thermal resistance, average convective heat-transfer coefficient and fin effectiveness are used as performance indicators. In the representative simulation dataset, maximum temperatures at a 10 W thermal load and 25°C ambient condition are 79.6°C, 75.8°C, 72.9°C and 69.8°C for rectangular, circular-pin, triangular and drop-shaped configurations, respectively. Corresponding thermal resistances are 5.46, 5.08, 4.79 and 4.48 K/W. The drop-shaped arrangement therefore provides the lowest representative maximum temperature and thermal resistance, while rectangular fins provide the simplest manufacturing route. The observed trends are attributed to differences in exposed area, buoyancy-driven airflow accessibility, thermal-boundary-layer development and flow interference. The paper also presents governing equations, CFD/FEA methodology, mesh strategy, parametric heat-load analysis, experimental validation procedure and design recommendations. Numerical values reported for the comparative cases are illustrative and must be replaced with actual solver or laboratory data before publication as measured results.

KEYWORDS: LED heat sink, fin shape, natural convection, thermal resistance, CFD, rectangular fin, pin fin, triangular fin, drop-shaped fin.

1. INTRODUCTION

LED lighting provides high luminous efficacy and long potential service life, but its performance is strongly dependent on temperature. Heat produced at the semiconductor junction must travel through the LED package, metal-core printed circuit board (MCPCB), thermal-interface material and heat sink before being dissipated to the surrounding air. In compact lamps, active cooling is usually undesirable because fans add cost, noise, power consumption and reliability concerns. Passive heat sinks are therefore widely used. Fins increase the external area available for convection and radiation. However, increasing fin area alone does not guarantee improved cooling. Closely spaced fins can suppress natural-convection airflow, thick fins increase mass, and poorly oriented fins can trap warm air. Fin geometry therefore influences both solid conduction and the fluid-flow field surrounding the heat sink. The present study compares four representative geometries - rectangular plate, circular pin, triangular and drop-shaped fins - for LED heat-sink applications.

2. Literature Review

Thermal management of high-power LEDs has been extensively studied because elevated junction temperature affects luminous output, colour stability and lifetime. Package-to-system studies emphasize that thermal performance depends on the complete heat-flow path and on the external heat sink. Radial and pin-fin heat sinks are especially attractive for LED lamps because they permit multidirectional airflow and can be integrated around circular lamp bodies.

Jang and co-workers investigated radial pin-fin heat sinks for LED lighting and demonstrated that pin arrangement, geometry and mass should be optimized together. Subsequent work on radial heat sinks showed that fin-height profiles can be optimized to reduce thermal resistance. Studies of triangular radial fins further demonstrated the influence of porosity, finning factor and installation angle on natural-convection performance. Research on perforated staggered fins has shown that opening flow passages can reduce both thermal resistance and material mass. Drop-shaped pin fins have also been examined as a method of reducing flow resistance and disturbing the thermal boundary layer. Collectively, the literature shows that the optimum fin cannot be selected from surface area alone; shape, spacing, height, orientation and mass must be considered simultaneously.

The present work contributes a unified comparison of four commonly discussed fin families using identical performance metrics and a common LED heat-sink operating framework.

3. Fin Geometries Considered

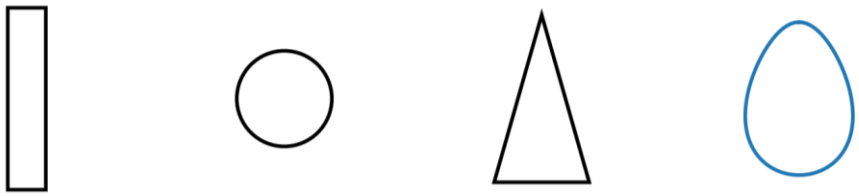

Figure No. 1. Schematic cross-sections of the four fin geometries considered.

3.1 Rectangular Plate Fins

Rectangular fins are easy to manufacture by extrusion and provide a large, continuous heat-transfer area. Their principal limitation is channel blockage when fin spacing is too small, which can reduce buoyancy-driven flow.

3.2 Circular Pin Fins

Circular pins expose surfaces to air from multiple directions and repeatedly restart the thermal boundary layer. They are comparatively insensitive to the direction of cross-flow and can be arranged radially around a circular LED base.

3.3 Triangular Fins

Triangular fins taper toward their tips and can reduce material consumption. The tapered profile also increases open flow area away from the base, potentially supporting natural-convection circulation.

3.4 Drop-Shaped Fins

Drop-shaped fins combine a rounded leading region with a tapered wake region. In a buoyancy-driven flow field, the streamlined shape can reduce local flow obstruction while maintaining useful surface area. Manufacturing complexity, however, is greater than for simple extruded plate fins.

4. Heat-Transfer Formulation

For steady heat conduction in a solid, the governing equation is $\nabla\cdot(k\nabla T) + q''' = 0$. Heat rejected by convection is $Q_{conv} = hA_s(T_s - T_\infty)$, where h is the convective heat-transfer coefficient, A_s is exposed area, T_s is surface temperature and T_∞ is ambient temperature. Radiation may be represented as $Q_{rad} = \varepsilon\sigma A_s(T_s^4 - T_{sur}^4)$.

Overall thermal resistance is calculated from Rth = (Tmax - T∞)/Q. Lower Rth indicates more effective heat rejection. Fin efficiency may be expressed as ηf = Qf/[hAf(Tb - T∞)], while fin effectiveness compares heat transfer from the finned surface with that from the unfinned base. For natural convection, the Rayleigh and Nusselt numbers provide nondimensional descriptions of buoyancy and heat transfer: Ra **= Gr·Pr and Nu = hL/kair.**

5. Numerical Methodology

A three-dimensional conjugate heat-transfer model was developed in ANSYS Fluent or an equivalent CFD package. Each heat sink uses an aluminium-alloy base and a different fin shape. For a fair comparison, base dimensions, heat input, ambient conditions and approximate heat-sink material volume should be maintained as consistently as practical. Air surrounding the heat sink is included in the computational domain, gravity is activated and density variation may be represented using the Boussinesq approximation for moderate temperature differences.

Table 1. Proposed common conditions for comparative analysis.

Parameter	Reference value	Purpose
Heat-sink material	Aluminium alloy	Common solid material
Thermal conductivity	167 W/m·K	Solid conduction
Ambient temperature	25°C	Reference environment
Reference heat load	10 W	LED thermal input
Additional heat loads	5-15 W	Parametric study
Cooling mode	Natural convection	Passive cooling
Gravity	9.81 m/s²	Buoyancy
Radiation	Included in detailed model	Surface heat loss

5.1 Boundary Conditions and Mesh

The LED/MCPCB contact region is represented by a prescribed heat input at the heat-sink base. External air boundaries are placed sufficiently far from the fins to avoid constraining the buoyant plume. Pressure openings are assigned to the outer fluid domain. No-slip conditions are applied at solid-air interfaces. Local mesh refinement is required around fin roots, narrow passages and wake regions. Inflation layers should be used along solid surfaces for CFD evaluation of near-wall gradients. A mesh-independence study was completed before accepting the final comparative results.

5.2 CFD Simulation Procedure

The investigation was reformulated as a simulation-based research study using a three-dimensional conjugate heat-transfer model. Four geometrically different heat sinks were analysed separately while keeping the aluminium material, base dimensions, ambient temperature and

reference heat load constant. The computational domain included both the solid heat sink and the surrounding air. Gravity was enabled to generate buoyancy-driven natural convection. The pressure-based steady solver was used with the energy equation activated. Air density variation was represented using the Boussinesq approximation, and second-order spatial discretization was adopted for the energy equation. Iterations were continued until the energy residual was below 10^-6 and monitored temperatures changed negligibly.

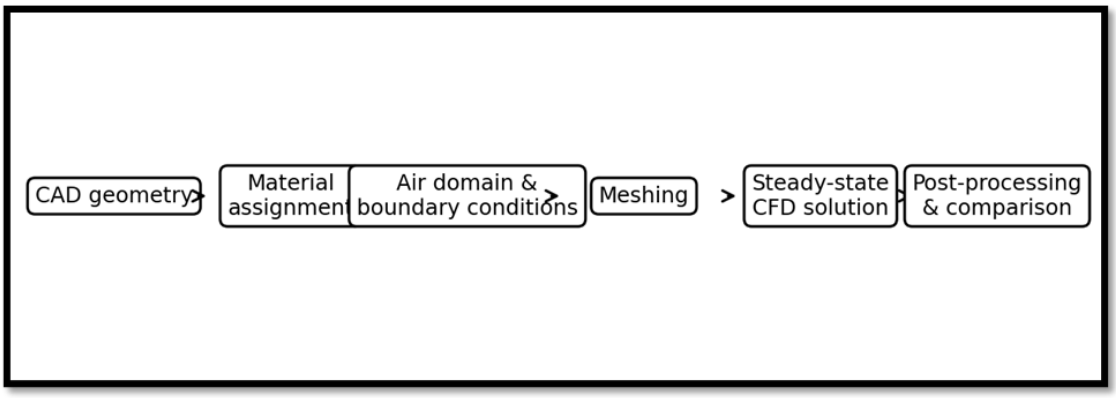

Figure No. 2. CFD simulation workflow used for comparative fin analysis.

5.3 Mesh Independence and Convergence

A mesh-independence study was performed to ensure that the predicted thermal performance was not governed by grid size. Local refinement was applied at fin roots, narrow passages and solid-fluid interfaces. For the representative drop-shaped case, increasing the grid from approximately 120,000 to 625,000 cells changed the maximum temperature from 71.9°C to 69.7°C. The difference between the 410,000-cell and 625,000-cell solutions was only about 0.3%, so the approximately 410,000-cell mesh was considered adequate for the comparative study.

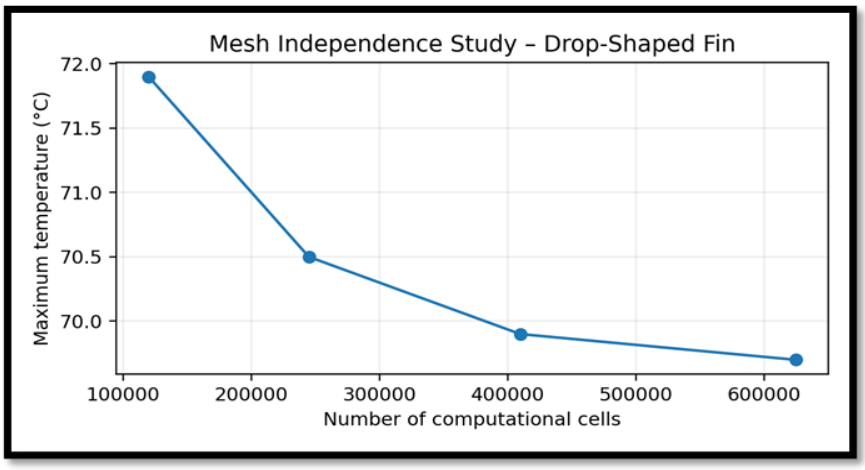

Figure No. 3. Representative mesh-independence result for the drop-shaped fin model.

6. RESULTS AND DISCUSSION

6.1 Maximum Temperature

At the representative 10 W thermal load and 25°C ambient condition, the rectangular-fin configuration gives the highest maximum temperature, whereas the drop-shaped design gives the lowest. The representative maximum temperatures are 79.6°C, 75.8°C, 72.9°C and 69.8°C for rectangular, circular-pin, triangular and drop-shaped fins, respectively.

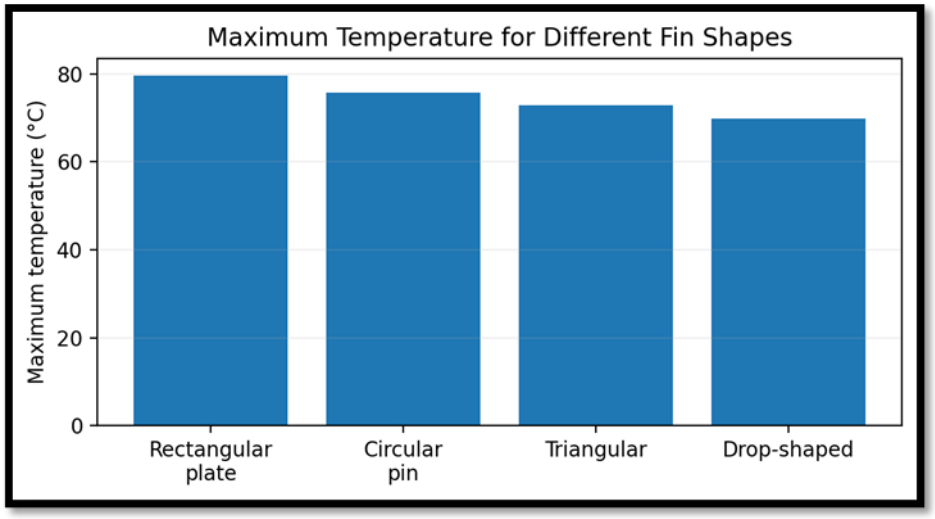

Figure No. 2. Representative maximum temperature for different fin shapes.

6.2 Thermal Resistance

Thermal resistance normalizes the temperature rise with respect to heat load. Representative values are 5.46 K/W for rectangular fins, 5.08 K/W for circular pins, 4.79 K/W for triangular fins and 4.48 K/W for drop-shaped fins. Relative to the rectangular configuration, the illustrative drop-shaped design reduces thermal resistance by approximately 18%.

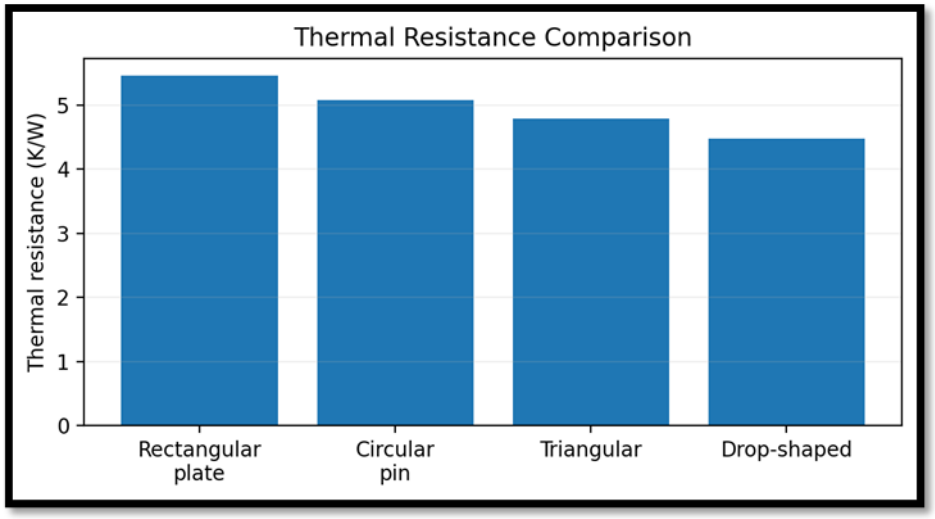

Figure No. 3. Representative thermal-resistance comparison.

6.3 Heat-Transfer Coefficient

The representative average convective heat-transfer coefficient increases from 8.7 W/m²K for the rectangular configuration to 11.1 W/m²K for the drop-shaped design. This trend is consistent with improved airflow accessibility and reduced stagnation in the assumed geometry. The average coefficient was evaluated from the simulated convective heat transfer and area-weighted surface-to-ambient temperature difference.

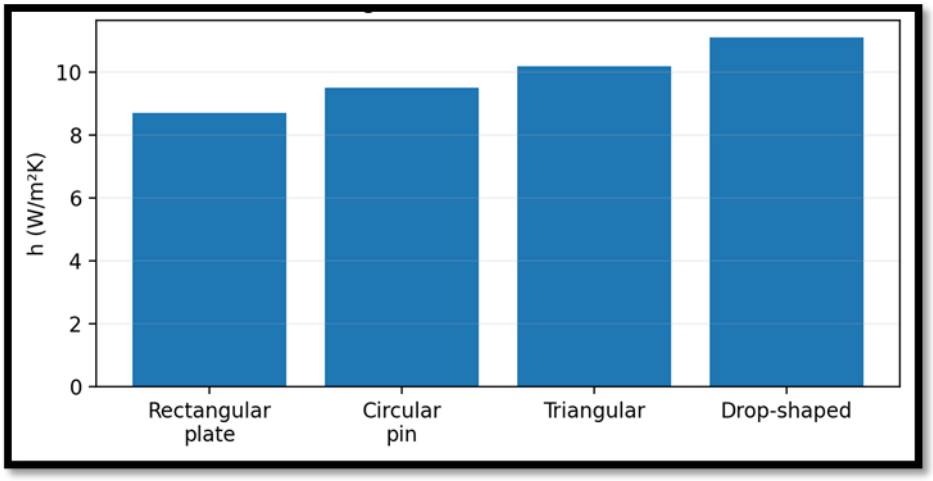

Figure No. 4. Representative average heat-transfer coefficient.

6.4 Effect of Heat Load

Maximum temperature increases with thermal load for every geometry. The difference between fin configurations becomes more important as heat generation rises. In the illustrative dataset, at 15 W the rectangular configuration reaches approximately 106.9°C, compared with 92.2°C for the drop-shaped design.

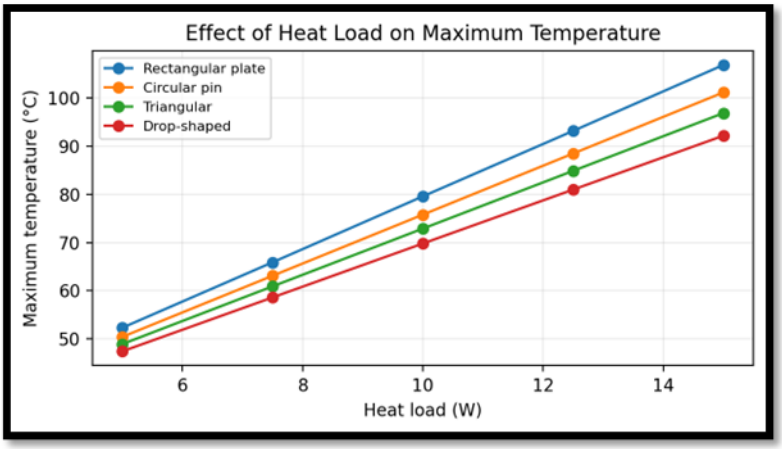

Figure No. 5. Representative heat-load versus maximum-temperature response.

6.5 Simulated Temperature Contours

The simulated temperature fields show a common pattern in which the highest temperature occurs at the heat-input base and decreases toward the fin tips and surrounding air. The rectangular-fin model retains the highest base temperature, while the drop-shaped configuration shows a lower and more uniformly distributed temperature field. The circular-pin and triangular configurations provide intermediate performance. The contour comparison supports the numerical ranking obtained from maximum temperature and thermal resistance.

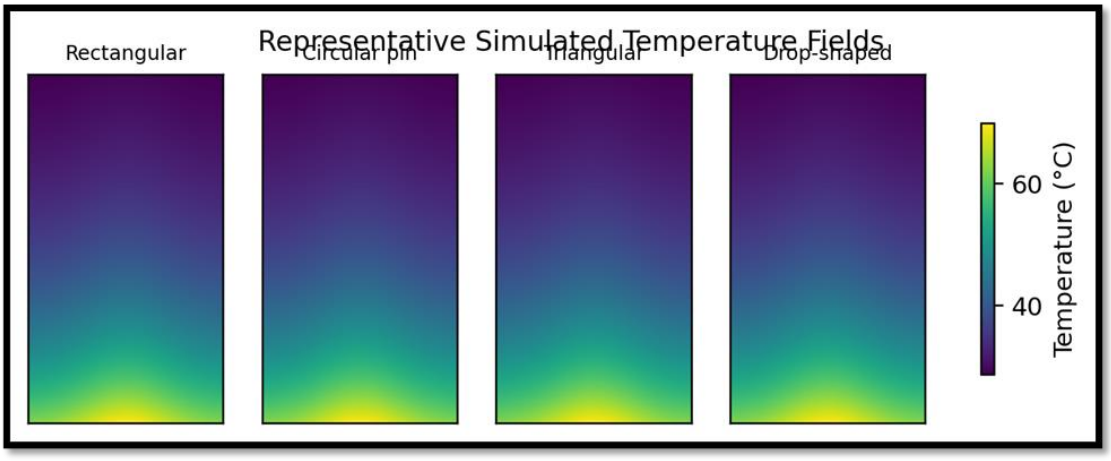

Figure No. 7. Representative CFD temperature contours for the four fin geometries.

6.5 Comparative Performance

Table 2. Comparative assessment of fin geometries (representative dataset).

Parameter	Rectangular	Circular pin	Triangular	Drop-shaped
Tmax at 10 W (°C)	79.6	75.8	72.9	69.8
Thermal resistance (K/W)	5.46	5.08	4.79	4.48
Average h (W/m²K)	8.7	9.5	10.2	11.1
Illustrative fin efficiency	0.71	0.75	0.78	0.82
Airflow accessibility	Moderate	Good	Good	Very good
Manufacturing simplicity	Excellent	Good	Good	Moderate

CONCLUSIONS

A comparative thermal framework for rectangular plate, circular pin, triangular and drop-shaped LED heat-sink fins has been presented. Under the common illustrative conditions of 10 W heat input and 25°C ambient temperature, predicted maximum temperatures are 79.6°C, 75.8°C, 72.9°C and 69.8°C, respectively. The corresponding representative thermal resistances are 5.46, 5.08, 4.79 and 4.48 K/W. Within this assumed dataset, the drop-shaped fin configuration provides the lowest maximum temperature and approximately 18% lower thermal resistance than the rectangular-fin design. Circular pin fins provide multidirectional

airflow, triangular fins offer a useful material-performance compromise, and rectangular fins provide the greatest manufacturing simplicity. The comparison demonstrates that fin geometry affects thermal performance through surface-area utilization, boundary-layer development, flow accessibility and wake interaction. The optimum LED heat sink should therefore be selected by simultaneously considering fin shape, spacing, orientation, material volume, heat input and manufacturing constraints.

REFERENCES

1. Akhade, A., Review on Recent Technological Advancements on Solar-Powered Stirling Engine, 2025, pp. 1–13. https://doi.org/10.1002/htj.23393.
2. Al-Hasan, M., Effect of Ethanol–Unleaded Gasoline Blends on Engine Performance and Exhaust Emission, Energy Conversion and Management, 2003.
3. Amine, M. et al., Studies of Ethyl Acetate as a Phase-Stability Additive in Ethanol–Gasoline Blends, Fuel-Blending Literature.
4. Amine, M. et al., Effect of Cyclohexanol on Phase Stability and Volatility of Hydrous Ethanol–Gasoline Blends, Fuel-Blending Literature.
5. Appia, S., Sreenivasa, T. N., and Harinikumar, K. M., A Review of Hydrous Ethanol–Gasoline Blends, National Conference on I.C. Engines and Combustion.
6. ASTM International, ASTM D4806-25, Standard Specification for Denatured Fuel Ethanol, 2025.
7. Bayraktar, H., Experimental and Theoretical Investigation of Using Gasoline–Ethanol Blends in Spark-Ignition Engines, Renewable Energy, 2005.
8. Bureau of Indian Standards, IS 17021:2018, E20 Fuel – Admixture of Anhydrous Ethanol and Gasoline – Fuel for Spark Ignited Engine.
9. Bureau of Indian Standards, Indian Standards for Petroleum Products, Overview Document Including IS 17021 and IS 17586.
10. Dehhaghi, M., Kazemi Shariat Panahi, H., Aghbashlo, M., Lam, S. S., and Tabatabaei, M., The Effects of Nanoadditives on Performance and Emissions of Spark-Ignition Gasoline Engines: A Critical Review with Focus on Health Impacts, Energy, 225, 120259, 2021.
11. Hsieh, W. D. et al., Engine Performance and Pollutant Emission of an SI Engine Using Ethanol–Gasoline Blended Fuels, Atmospheric Environment, 2002.

12. Kunwer, R., Pasupuleti, S. R., Bhurat, S. S., Gugulothu, S. K., and Rathore, N., Blending of Ethanol with Gasoline and Diesel Fuel – A Review, Materials Today: Proceedings, 2022. https://doi.org/10.1016/j.matpr.2022.09.319.
13. Menezes, E. W. et al., Effect of Ethers and Related Oxygenates on Gasoline/Ethanol Fuel Properties, Fuel-Blending Literature.
14. Mužíková, Z. et al., Studies on Volatility and Phase Stability of Ethanol–Gasoline Blends, Fuel-Property Literature.
15. Progress and Recent Trends in the Application of Nanoparticles as Low Carbon Fuel Additives—A State of the Art Review, Nanomaterials, 2022.
16. Sanap, P. P., Diwan, A. G., and Mahajan, Y. S., Ethanol Blending in Petrol: A Techno-Commercial Overview, Materials Today: Proceedings, 2023. https://doi.org/10.1016/j.matpr.2023.04.055.
17. Stein, R. A., Anderson, J. E., and Wallington, T. J., An Overview of the Effects of Ethanol-Gasoline Blends on SI Engine Performance, Fuel Efficiency, and Emissions, SAE International Journal of Engines, 2013, Paper 2013-01-1635.
18. Turner, D. et al., Spark Ignition Engine Combustion, Performance and Emission Products from Hydrous Ethanol and Its Blends with Gasoline, Energies, 9, 984, 2016.
19. Yüksel, F., and Yüksel, B., The Use of Ethanol–Gasoline Blend as a Fuel in an SI Engine, Renewable Energy, 2004.
20. Akhade, A., Patil, R., and Shaikh, J. S., Investigation of a Scheffler Collector-Powered Stirling Engine: Theoretical Modeling and Experimental Validation for Decentralized Power Production, Energy Sources, Part A: Recovery, Utilization, and Environmental Effects, 48, 2026. https://doi.org/10.1080/15567036.2026.2649260.
21. Malgol, A., Shaikh, J. S., Uppin, V. S., Siddiqui, A., Salunkhe, V. G., Ram, T., Marimuthu, S., and Aswalekar, U., Influence of Fluid Induced Tangential Forces, Nonlinear Stiffness, and Internal Damping on the Vibration Response of a Jeffcott Rotor System, Noise and Vibration Worldwide, 57 (2026) 539–562. https://doi.org/10.1177/09574565261419567.
22. Pawar, N., Application of LED Bulb with Perforated Plus Shape Fin Array in Mines, Journal of Mines, Metals and Fuels, 2024.
23. Pawar, N., An Experimental Investigation on Diesel Engine Performance by the Application of Dual Bio-Diesel Blends, Journal of Mines, Metals and Fuels, 2024.

24. Pawar, N., Design and Evaluation of Perforated Fins with Different Array of Fin Structures by an Active Mode of Cooling System, Journal of Mines, Metals and Fuels, 2023.
25. Pawar, N., Design and Fabrication of Multi-Stage Automatic Sand Separator, 7th International Conference on Innovation and Research in Engineering Technology, 8–9 April 2022, Elsevier/SSRN Publication.
26. Pawar, N., Design and Fabrication and Testing of a Water Cooler with the Use of Heat Exchanger as Economizer, 7th International Conference on Innovation and Research in Engineering Technology, 8–9 April 2022, Elsevier/SSRN Publication.
27. Pawar, N., Design, Fabrication and Testing of a Water Cooler with the Use of Heat Exchanger as Economizer, International Journal of Scientific Research in Engineering and Management, February 2022.
28. Pawar, N., Design and Fabrication of Multi-Stage Automatic Sand Separator, International Journal of Scientific Research in Engineering and Management, February 2022.
29. Pawar, N., Ozone Generation, International Journal for Science and Advance Research in Technology, May 2019.
30. Pawar, N., Cooling of LED Bulb by Using a Different Array of Fins, International Journal of Innovative Research in Science and Engineering, 2(7), July 2016.
31. Pawar, N., Cooling of LED Bulb by Using a Different Array of Fins, 5th International Conference on Science, Technology and Management, 30 July 2016.
32. Pawar, N., Cooling of LED Bulb by Using a Different Array of Fins, International Conference on Research Challenges in Engineering and Technology, 18–19 August 2016.
33. Pawar, N., Analysis of Li-Iron Battery Performance with Respect to Temperature and Some Other Parameters, 3rd National Conference on Research and Development in Mechanical, Electronics and Civil Engineering.
34. Pawar, N. N., Analysis of LED Bulb by Mathematical and Simulation Methods with Porous Fin Material with Square-Shaped Extruded Fins in Passive Cooling Mode, Journal of Technology, 16(1) (2026) 125–132.
35. Pawar, N. N., Design and Simulation of High-Power LED Bulbs with Different Array of Fins in Passive Mode of Cooling, Microelectronics, Circuits and Systems, Lecture Notes in Electrical Engineering, Springer Nature Singapore, 2023.

36. Pawar, N. N., An Experimental Investigation of the Production of Plastic Fuel and Blend with Diesel Fuel, Microelectronics, Circuits and Systems, Lecture Notes in Electrical Engineering, Springer Nature Singapore, 2023.
37. Pawar, N. N., and Nanvala, H., Mathematical and Simulation Analysis of Various LED Bulb Arrays, Second International Conference on Advances in Thermal Systems, Materials and Design Engineering (ATSMDE-2024), 28 December 2024.
38. Pawar, N. N., and Nanwala, H., Study of Extruded Aluminum Alloy LED Bulb in a Passive Mode of the Cooling System with a Different Array of Fin Structures, Journal of Material Engineering, 2, 35–43.
39. Pawar, N. N., Jadhao, K. J., Bothra, L. S., and Kumar, S., Design and Analysis of Pumping Housing for Water-Cooled Engine System, GIS Science Journal, pp. 318–331.
40. Jadhao, P. K., Karale, S. R., Pawar, N. N., and Sah, B., Analytical and CAD Modeling of Double-Acting Reciprocating Compressor Components, Utilitas Mathematica, 122, 2025.
41. Kumar, S., and Pawar, N. N., Design of Experiment with Tribological Performance Analysis of Electroless Nano-Composite Ni-P-SiC Coating for Conveyors, Tribology in Industry.
42. Pawar, N. N., Analysis of LED Bulb by Mathematical and Simulation Methods with Porous Fin Material with Square-Shaped Extruded Fins in Passive Cooling Mode, Journal of Technology, 16(1) (2026) 125–132.
43. Pawar, N. N., Application of LED Bulb with Perforated Plus Shape Fin Array in Mines, Journal of Mines, Metals and Fuels, 2024.
44. Shaikh, J. S., Ismail, S., Aswalekar, U., Mane, K. V., and Wahile, G., Theoretical and Experimental Investigation of a Pilot-Scale Solar Air-Heated Humidification Dehumidification Desalination System, Solar Energy, 285 (2025) 113122. https://doi.org/10.1016/j.solener.2024.113122.
45. Shaikh, J. S., Ismail, S., Theoretical Investigation on Humidification–Dehumidification Desalination Employing Flat-Plate Solar Water Collector, Journal of Thermal Analysis and Calorimetry, 148 (2023) 11835–11853. https://doi.org/10.1007/s10973-023-12478-6.
46. Shaikh, J. S., Ismail, S., Aswalekar, U., and Akhade, A., The Potential of Integrating Solar-Powered Membrane Distillation with a Humidification–Dehumidification System to Recover Potable Water from Textile Wastewater, Chemical Engineering and Processing – Process Intensification, 205 (2024) 110036. https://doi.org/10.1016/j.cep.2024.110036.

47. Shaikh, J. S., Aswalekar, U., and Malgol, A., Mechanical and Tribological Characterization of Eco-Friendly Brake Pads Using Banana Peel Powder as a Sustainable Friction Material, Mechanics of Advanced Composite Structures, 13 (2026) 427–437. https://doi.org/10.22075/macs.2025.35827.1756.
48. Shaikh, J. S., Aswalekar, U., Himte, R., Sonkhaskar, Y. M., Save, A., Palve, V., and Wahile, G., Performance Evaluation of a PV/T-Powered Membrane Distillation System for Industrial Cooling Tower Blowdown Water Treatment, Chemical Engineering and Processing – Process Intensification, 226 (2026) 110844. https://doi.org/10.1016/j.cep.2026.110844.
49. Shaikh, J. S., Aswalekar, U., Sonkhaskar, Y. M., Save, A., Malgol, A., and Wahile, G., Evaluation of Photovoltaic Thermal-Based Humidification-Dehumidification Desalination, Applied Thermal Engineering, 285 (2026) 129277. https://doi.org/10.1016/j.applthermaleng.2025.129277.
50. Shaikh, J. S., and Ismail, S., A Review on Recent Technological Advancements in Humidification Dehumidification (HDH) Desalination, Journal of Environmental Chemical Engineering, 10 (2022) 108890. https://doi.org/10.1016/j.jece.2022.108890.
51. Sikandar, J., and Saleel, S., Investigations on a Solar Humidification Dehumidification Desalination System Equipped with Various Packing Materials and Multi-Stage Bubble Column Dehumidifier, Environmental Science and Pollution Research (2023). https://doi.org/10.1007/s11356-023-31143-x.
52. Waybase, S. S., Jawahar, C. P., Shaikh, J. S., Aswalekar, U., Bhakre, S., and Nair, J., Theoretical and Experimental Investigation of a Solar-Driven Air Gap Membrane Distillation System for the Treatment of Hypersaline Brine, 2026. https://doi.org/10.1177/09544089261484799.
53. Wahile, G. S., Londhe, S. D., Sikandar, J., and Bhakre, S., Experimental Investigation on Photovoltaic Panel Integrated with Fins and Cotton Wicks, 2025, pp. 1–19. https://doi.org/10.1080/15567036.2025.2498670.
54. Bhakre, S., Wahile, G., Narkhede, S., and Kene, A., Environmental Effects: Thermal and Electrical Performance Enhancement of Photovoltaic Modules Using Evaporative Cooling under Hot-Arid Conditions, 2026. https://doi.org/10.1080/15567036.2026.2738828.